Journal of KSNVE, Vol. 8, No. 1, pp. 57~74, 1998.

〈Orignal Paper〉

Dynamic Analysis of Design Data for Structural Lap Joint

LAP 구조물 결합부의 설계치 확보를 위한 동역학적 해석

Seong-Ho Yun*
윤 성 호

(Received June 10, 1997 ; Accepted November 13, 1997)

Key Words : Joint Flexibility (결합 유연성), Dynamic Stiffness (동강성 계수), Nonlinearity Vibration Test (비선형 진동시험), Modal Parameter Sensitivity (모달 매개변수 민감도), Finite Element Modeling (유한요소 모델링).

ABSTRACT

This paper is concerned with a combination of experimental and analytical investigation aimed at identifying modeling errors, accounted for the lack of correlation between experimental measurements and analytical predictions of the modal parameters for lap joint panels. A nonlinearity vibration test methodology, initiated from the theoretical analysis, is suggested for measurements of dynamic stiffnesses in a lap joint using the rivet fastener. Based on the experimental evidence on discrepancies between measured and predicted frequencies, improved finite element models of the joint are developed using PATRAN and ABAQUS, in which the beam element size is evaluated from the joint stiffnesses readily determined in the test. The beam element diameter as a principal design parameter is tuned to match experimental results within the evaluated bound value. Frequencies predicted by the proposed numerical model are compared with frequencies measured by the test. Improved predictions based on this new model are observed when compared with those based on conventional modeling practices.

요 약

구조체 연결부위에서 미지의 결합강성으로 인하여, 실험과 유한요소법으로 구한 모달 매개변수들은 종종 일치하지 않는다. 본 논문은 실험으로 추출된 동특성 데이타에 근거하여, 해석적인 방법을 통해 새로운 모델링 방법을 제시하고 있다. 대표적인 연결방법으로 리벳을 이용한 Lap 이음보에서 동강성을 측정하기 위한 비선형 진동실험이 제안되었으며, 이를 Lap 이음판에 적용하기 위하여 동강성에 해당하는 설계변수로서 빔요소를 도입하였다. 이 유한요소 모델링은 범용 패키지인 PATRAN과 ABAQUS를 사용하였으며, 빔요소의 직경을 실험치의 고유진동수와 일치하도록 조절함으로써 직경의 최적치 경향을 관찰하였다. 제시된 모델링 기법과 기존의 모델링 기법으로 얻은 결과치들을 실험치와 비교하였다.

1. Introduction

Most actual mechanical structures are composed of many parts connected to one another by various type of joints. The study on these connected structures dynamically subjected to various forces is an important

* Member, Korea Railroad Research Institute

remaining challenge in identification of joints and development of their structural dynamic models. Some analytical works have been performed on idealization of the joint[1,2]. In an attempt to establish the numerical model, many researchers have been designing tools for linking finite element analysis results with experimental results. These studies have in general focused on either experimental or analytical method but rarely both. It is usually recognized that each analysis method has its own inherent inaccuracies or drawbacks[3]. Thus, it often can create arguments as to which set of results is more reasonable.

Some approaches[4,5] have been limited to the deformation analysis for the connected structures under a static tensile loading. In an operational loading state, however, modeling of jointed regions is a difficult task when the fastener is rocked and tilted due to nonsymmetry and hole crushing of the joint. Correspondingly, the vibration cycle exciting the jointed structure causes the flexible fastening situation, and thereby physically results in stiffness loss or damping increase in the joint. Until recently, the numerical idealization of the joint has been executed in such an empirical manner that the fastener flexibility is determined by the margin of safety using engineering handbooks.

A clear evidence of incorrect predictions for the stiffness and the damping magnitude in the joint was reported in the design of semi-monocoque vehicle structures[6,7]. By reusing much of the statics analysis model for the dynamics analysis, secondary and nonstructural items attached to the skin or deck have been conservatively modeled as rigid. Connection flexibility between members has been ignored for the dynamic analysis. There has been no complete rationale on which experimental extractions of dynamic characteristics in flexible joints are based.

Verification of finite element models using experimental data is a common practice in many engineering applications. Thus, this verification process is centered on vibration test results, requiring the model to produce reliable predictions with confidence. Correlation of analytical predictions to experimental measurements is usually demonstrated on comparison of modal parameters, primarily natural frequency and mode shape, rather than comparison of mass and stiffness matrices. In a large scale structure, these matrices in the finite element model contain a larger number of DOF than the responses measured by the test program. Moreover, matrix elements can not be explicitly extracted on the basis of vibration tests. A test/analysis model should be one reduced to the same DOF as instrumented in the correlation analysis. This experimental model is used as a benchmark test to provide a direct link for correlations between the analytically predicted and experimentally measured modal parameters[8].

As an example of both experimental and numerical illustrations, the single lap joint using the rivet will be demonstrated on an assessment of applicability to the standard test method. Prior to building test samples, this model should represent a typical lap joint as an integral part of the entire structure. An important step to the improved modeling process is to identify major contributors to the lack of experimental/analytical correlations. Subsequently, the idealized model of the jointed area needs adjustment to the conservative modeling assumptions. More realistic modeling of the joint damping is also responsible for the joint flexible capability. Hence damping effects in joints are required to observe experimentally. This paper will focus on prediction capabilities of modal parameters in such a combined experimental and numerical manner that modeling errors can be

identified for the design process improvement. First, an analytical model of the beam with a midspan joint will be studied to examine the effects of translational and torsional stiffnesses using spring constants. Second, a vibration test procedure will be proposed to measure stiffnesses, so that these values can subsequently be implemented in the finite element model of the corresponding joint. Third, a more realistic idealization methodology will be illustrated for the model of the joint, based on experimentally determined joint stiffness. The rivet as a fastener is used in this study.

2. Theoretical Approach

The conceptual basis on the forthcoming approach for the prediction of the stiffness in a joint is to insert a fastener at tips of two cantilever beams and then to vary the magnitude of the stiffness to represent the joint property. Modal properties of the clamped-clamped beam with a midspan joint are apparently different from those obtained from the corresponding beam with no joint. On the basis of reference modal parameters, sensitivities to modal parameters of the jointed beam can be investigated by changes in stiffness.

2.1 Elastic Constraints

For odd-numbered (or *symmetric*) modes of the clamped-clamped reference beam with no joint, maximum moments are dominated with no shear force at the midspan; on the contrary, for even-numbered (or *anti-symmetric*) modes, maximum shear forces exist with no moments at the midspan. Accordingly, slopes for symmetric modes and deflections for anti-symmetric modes vanish at the midspan, respectively.

These two groups of dynamic phenomena can be described by imposing elastic constraints at tips of two cantilever beams

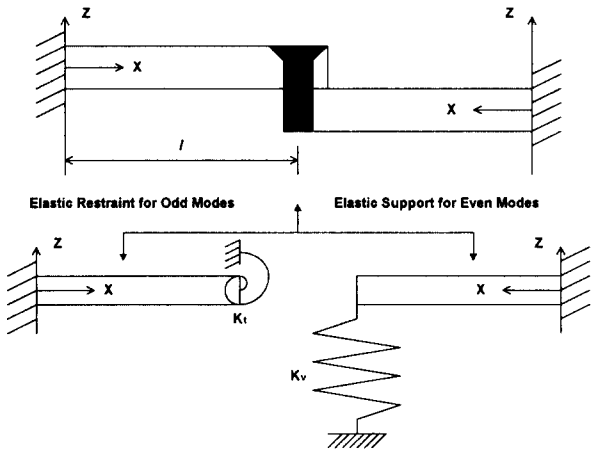

Fig. 1 Two groups of the dynamic characteristic for a single lap joint.

of length ℓ obtained by cutting the clamped-clamped beam of length 2ℓ, as shown in Fig. 1 Symmetric modes of this reference beam can be obtained by an introduction of infinite restraint to the tip of the cantilever beam using a torsional spring k_t whereas anti-symmetric modes of the corresponding reference beam can be obtained by imposing infinite support on the tip of the cantilever beam using a translational spring k_v.

2.2 Eigen Analysis

The dynamic behavior of each beam is assumed as the small transverse vibration of the cantilever beam. Referring to Fig. 1, their associated boundary conditions are as follows:

for the tip torsional restraint:

$$@x=0:\ \Phi(0)=0,\ \Phi'(0)=0,$$
$$@x=\ell:\ \Phi''(\ell)+\frac{k_t}{EI}\Phi'(\ell)=0,\ \Phi'''(\ell)=0 \qquad (1\text{-a,b})$$

for the tip translational support:

$$@x=0:\ \Phi(0)=0,\ \Phi'(0)=0,$$
$$@x=\ell:\ \Phi'''(\ell)-\frac{k_v}{EI}\Phi(\ell)=0,\ \Phi''(\ell)=0 \qquad (2\text{-a,b})$$

where EI is the bending stiffness of the beam. The notation $(.)'$ denotes a derivative

with respect to x and $\Phi(x)$ the transverse vibration amplitude.

Next step is to solve these two sets of eigen problems under assumptions made on the Euler- Bernoulli beam. Small vibration deflections are expressed as the following general equation:

$$\Phi_i(x) = a_1 \sin\beta_i x + a_2 \cos\beta_i x + a_3 \sinh\beta_i x + a_4 \cosh\beta_i x \quad (3)$$

where values of β_i and three of the four constants of a_1, a_2, a_3 and a_4 are determined from the above four boundary conditions. For a given m, mass per unit length of the beam, β_i is defined as

$$\beta_i^4 = \frac{m\omega_i^2}{EI} \quad (4)$$

where ω_i is the angular frequency for the i^{th} mode.

Setting the determinant equal to zero with respect to the above four constants yields the following natural frequency equations:
for the tip torsional constraint:

$$\frac{G}{r_i}(\sin r_i \cosh r_i + \cos r_i \sinh r_i) + 1 + \cos r_i \cosh r_i = 0, \quad (5)$$

for the tip translational constraint:

$$\frac{K}{r_i^3}(\sin r_i \cosh r_i - \cos r_i \sinh r_i) + 1 + \cos r_i \cosh r_i = 0, \quad (6)$$

where $r_i(=\beta_i \ell)$ is an infinite number of eigen values, G is the nondimensional torsional stiffness and K is the nondimensional translational stiffness, defined as

$$G = \frac{k_t \ell}{EI} \quad (7)$$

and

$$K = \frac{k_v \ell^3}{EI}. \quad (8)$$

If the beam is free at the tip, which is identical to the case of the cantilever beam, only the last two terms remain in the natural frequency equations (5) and (6).

With only translational stiffness K increased to infinity at the tip of the cantilever beam of length ℓ, their vibration modes approach the anti-symmetric modes of the clamped-clamped beam of length 2ℓ, whereas symmetric modes of the clamped-clamped beam of length 2ℓ can be obtained with only torsional stiffness G increased to infinity at the tip of the cantilever beam of length ℓ.

3. Modal Parameter Sensitivities

Equations (5) and (6) provide a spectrum of natural frequencies by varying the value of stiffness K and G, respectively.

Furthermore, it is possible to acquire modal parameter sensitivities in terms of natural frequency and mode shape based on those of the reference beam. At first natural frequency sensitivities will be computed and then mode shape sensitivities will be investigated in terms of tip deflection.

3.1 Natural Frequency Sensitivity

In both cases of tip torsional restraint and tip translational support, natural frequency sensitivities were investigated by increasing one order of magnitude in a range of stiffness G and K from 10^{-10} to 10^{10} as shown in Figs. 2 and 3, respectively. The three lowest natural frequencies were obtained as a function of nondimensional spring constant. In both plots, natural frequency bases were obtained by imposing infinite spring stiffness at tips of the double cantilever beam.

In the sensitivity computation, the sensitivity is set to 0 % when the measured parameter is equal to the base value. Natural frequencies are very sensitive to the nondimensional stiffnesses, G and K, between 10^{-1} and 10^{4} For flexibilities below 10^{-1} in nondimensional stiffness, sensitivities become saturated close

to the case of the cantilever beam. Also, for too rigid joint with flexibilities above 10^4, variations of natural frequencies are almost close to the case of the clamped-clamped beam with no joint. As a result, dynamic responses caused by the joint flexibility under operational loadings is expected to be produced between 10^{-1} and 10^4 in nondimensional stiffness.

3.2 Mode Shape Sensitivity

Following eigen functions associated with their tip constraints are produced by eigen solutions as mentioned in the previous section:

for the tip torsional constraint:

$$\Phi_i(x) = a_4[\cosh\beta_i x - \cos\beta_i x - \frac{\sinh r_i - \sin r_i}{\cosh r_i + \cos r_i}(\sinh\beta_i x - \sin\beta_i x)], \quad (9)$$

for the tip translational constraint:

$$\Phi_i(x) = a_4[\cosh\beta_i x - \cos\beta_i x - \frac{\cosh r_i + \cos r_i}{\sinh r_i + \sin r_i}(\sinh\beta_i x - \sin\beta_i x)], \quad (10)$$

where a_4 is the undetermined coefficient of the mode shape. For both elastic constraints,

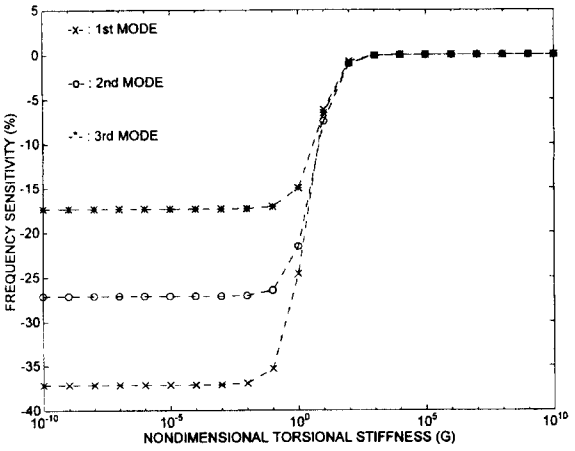

Fig. 2 Natural frequency sensitivities due to the tip torsional stiffness.

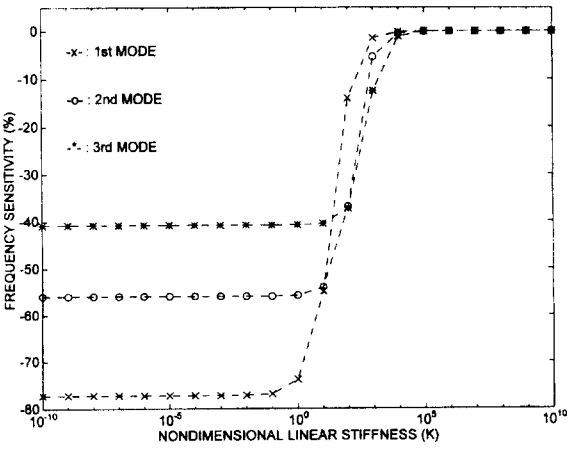

Fig. 3 Natural frequency sensitivities due to the tip translational stiffness.

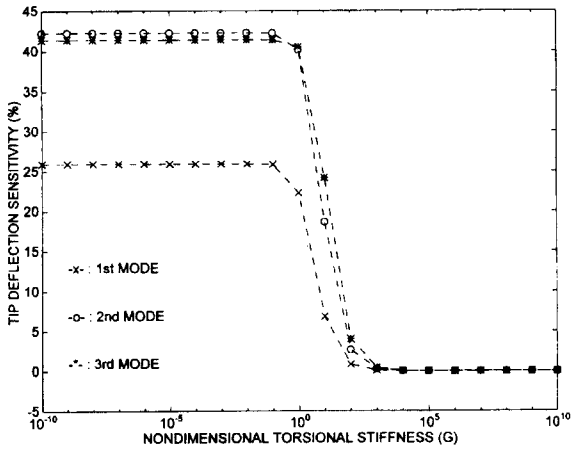

Fig. 4 Tip deflection sensitivities due to the tip torsional stiffness.

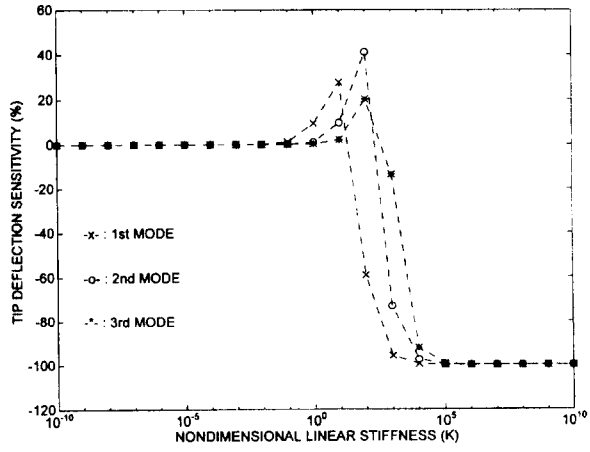

Fig. 5 Tip deflection sensitivities due to the tip translational stiffness.

the mode shape equation is of the same form as that of cantilever beam which in fact has free elastic constraints. However, the eigen value r_i is governed by the nondimensional spring stiffness G or K defined in equations (7) and (8).

Sensitivities to mode shapes can be also observed as a function of stiffness K and G, respectively. In comparing mode shapes given in equations (9) and (10) with the coefficient a_4 set to a constant, the reference amplitude due to torsional constraint was set as the tip amplitude for an infinite torsional spring stiffness. Similarly, the reference amplitude due to translational constraint was chosen as the tip amplitude for a zero translational spring stiffness. One convenient way of comparing each mode with the reference mode is to investigate its sensitivity at the tip, where deflections for each mode with infinite torsional and translational stiffness becomes maximum and zero, respectively.

Accordingly, tip deflections due to torsional restraint in Fig. 4 are normalized by midspan deflections of the clamped-clamped reference beam, and tip deflections due to translational support in Fig. 5 are scaled on the basis of those of a cantilever beam. In both cases, very sharp changes in tip deflection sensitivity occur approximately between 10^{-1} and 10^{4} in stiffness, G and K, respectively. In particular, there exist peak values of sensitivities for anti-symmetric modes around 10^{1} to 10^{3} in stiffness K. Tip deflections above 10^{4} in stiffness G are close to maximum deflections of the clamped-clamped reference beam. However, tip deflections below 10^{-1} in stiffness K and G converge to those of the cantilever beam. Tip deflections become zero for very rigid joints above 10^{4} in stiffness K. These physical phenomena are readily observed for the investigation of natural frequency sensitivities in extreme cases of stiffnesses.

4. Proposed Test Program

The experiment involves reference tests for sensitivity observations of modal parameters as well as calibrations of excitation force levels for a consistent test environment. In particular, the reference test is used to generate base values for the tip deflection sensitivity because the vibration amplitude magnitude depends on the excitation force level. Figure 6 shows the shaker test setup to control excitation forces, as well as the impact hammer test setup.

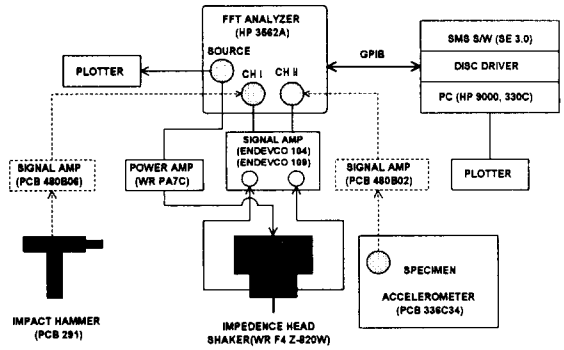

Fig. 6 The schematic diagram of a combination of impact hammer and shaker test setups.

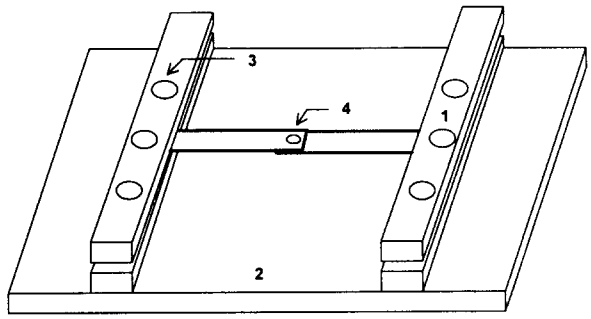

1. Solid steel bar : 50.8 mm x 101.6 mm x 381.0 mm, 15.42 kg/each
2. Base steel bar : 381.0 mm x 1016.0 mm x 25.4 mm, 77.56kg
3. Bolt diameter : 15.88 mm
4. Rivet diameter : 6.35 mm

Fig. 7 The experimental fixture for the clamped-clamped boundary condition.

4.1 Test Fixture

The supporting fixture in Fig. 7 was built massive enough to extract information regarding the structure of interest, not the supporting structure. The first few modes for jointed panels were isolated far from the fundamental mode for this fixture with a Clamped-Free-Clamped-Free (*CFCF*) boundary condition. The actual sample weighs 0.635 kg, as compared with the whole fixture weight over 135 kg. Four steel bars are used to clamp test samples by means of six 15.88 mm bolts. A base steel plate supports the entire assembly. For both linear and nonlinear vibration tests, the test setups were built as a combination of the impact hammer and shaker tests, depicted in Fig. 6.

4.2 Test Sample

The reference test for the extraction of joint properties needs two simple beams. The first sample is the beam of length 2ℓ = 406.40 mm clamped along both sides, denoted *CC* for a later reference. The second is the beam of length ℓ = 203.20 mm clamped along one side and free along the other, denoted *CF*. The single lap joint beam was made using a rivet fastener of diameter D = 6.35 mm located at midspan of double *CF* with length ℓ = 219.50 mm, and denoted *LRV*. All samples have the same width w = 22.86 mm and thickness t = 2.29 mm. The rivet's head is tapered and countersunk for a flush installation. Aluminum (Al *5052*) used as test specimen material has the following nominal properties: Young's modulus $E = 7.136\times10^9$ kg/m^2, Poisson's ratio ν = 0.33 and density $\rho = 2.685\times10^3$ kg/m^3. In a purpose of application to lap joint panels, one sample without joints was made the rectangular plate with 406.40 mm long along the two free edges and 254.00 mm wide along the two other clamped edges, and denoted *CFCF* for later reference. Typical lap joint panels were constructed using rivet fasteners as shown in Fig. 8. Width of disjointed main panels is 254.00 mm along two clamped edges in the *CFCF* boundary fixture and length is 203.20 mm along two other free edges. Two kinds of sample were tested according to the number of rivets with the same lap splice width $6D$: 4 rivets marked as '•' in Fig. 8 were employed and then 6 rivets marked as '○' were added to employ 10 rivets. Each corresponding sample will be denoted using the notation, *L#*, where *L* stands for Lap joints and # the number of

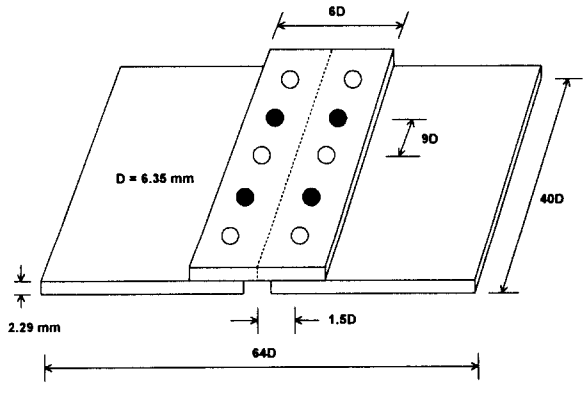

Fig. 8 The test sample for typical lap joint panels.

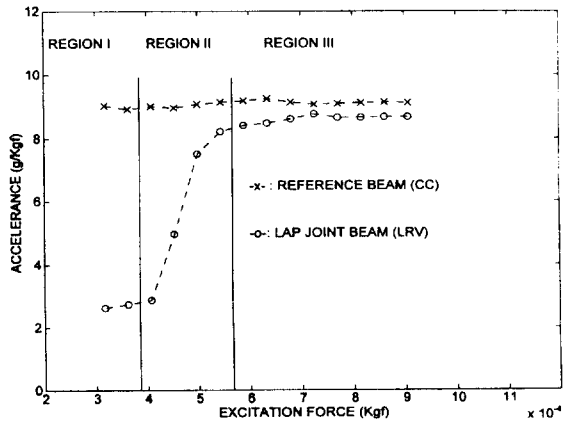

Fig. 9 The choice of excitation force levels in the first mode for consistency to tests of the jointed beam.

rivet to be fastened. For example, *L*10 indicates a lap joint with a 6*D* lap width fastened 10 rivets.

4.3 Excitation Force Calibration

Excitation force levels must be chosen properly to assure that the connected structure is actually excited in its true linear range. The choice of the excitation force level is needed for consistency of vibration tests for reference beams and the jointed beam. The force level is increased until there is no change in the transfer function for different force levels.

Figure 9 presents accelerances in g/kgf versus force level in kgf for the transfer accelerance which was measured from excitation forces using the shaker at location 19.05 mm off the clamped support and the acceleration *g* at the midspan location. This plot shows that excitation forces for the first mode of the *LRV* beam actually consist of three main regions, but the reference *CC* beam maintains a constant accelerance over the given excitation level. In the first force level area (Region I), the force level is so low that the friction force in the joint is significant. As the force level is increased (Region II), the friction force in the joint continues to reduce in magnitude causing a nonlinear relationship of accelerance versus force level. The third one (Region III) is the true linear region consisting of constant values of accelerance for changing values of force levels. This physical phenomenon, termed as ankylosis[9], occurs where the friction force in the joint has been reduced to a constant value. In other words, the friction force in the joint in the first two regions is too large to be overcome by the excitation force and tests yield variable accelerances. In all tests excitation forces were selected at about 6.8 $\times 10^{-4}$ kgf.

5. Preliminary Test Result

Two criteria will be used to evaluate correlations of the experimental/analytical results in the present work: natural frequency discrepancy and Modal Assurance Criterion (MAC). The first criterion is used to detect frequency errors produced by the finite element model. The second indicates the accuracy of mode shapes predicted by the corresponding model. In addition, the role of measured damping levels will be discussed.

5.1 Linearity Test

The first step is to verify test repeatability associated with reciprocity or linearity using the *CFCF* panel. It is because a standard boundary condition should be the

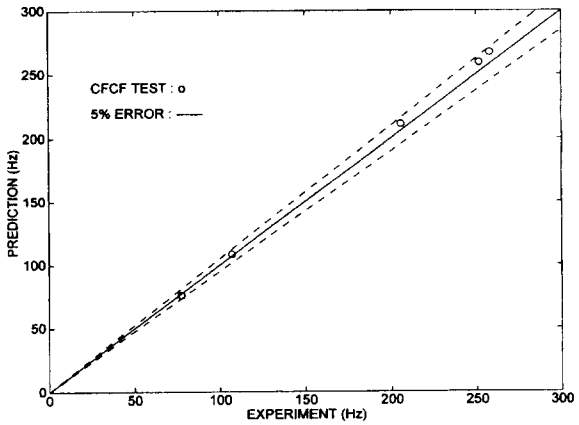

Fig. 10 Correlation between measured and predicted frequencies for the CFCF panel.

Table 1 The MAC matrix for the *CFCF* panel.

Mode	1	2	3	4	5
1	0.92	0.02	0.00	0.00	0.26
2	0.00	0.98	0.00	0.00	0.00
3	0.00	0.00	0.98	0.00	0.00
4	0.00	0.00	0.00	0.98	0.00
5	0.11	0.00	0.00	0.00	0.99

consistent test environment for the lap joint panels under test. Test results of the first five natural frequencies for the *CFCF* panel using the hammer test were compared with analytical results using the commercial FEM package, PATRAN and ABAQUS [10,11].

Figures 10 shows an excellent correlation between experimental measurements and analytical predictions. Errors are in a range of less than 2 %. Measured deflections for the corresponding five modes were compared with predicted deflections. MAC values were computed into the (5×5) matrix in Table 1 where the row modes are extracted from analytical results and the column modes from the modal testing data. The values on the diagonal in the MAC matrices are close to unity. This implies that the measured residue vectors are consistent with their computed mode shapes. Measured damping levels for the *CFCF* panel remained below 1 % critical, as compared with 0 % damping assumed in the analytical approach. Thus, the damping level has a little effect on natural frequencies. Three modal parameters show an excellent correlation and the *CFCF* boundary condition assures a consistent test environment for test articles using the shaker test.

5.2 Nonlinearity Test

The dynamic response of fastened structures is influenced by the nonlinear behavior which may be generated by the hole clearance and relative displacements between structural members. In the impact hammer test, infinitesimal amplitudes are measured by a very low level of excitation force. However, if a larger excitation force is applied to the jointed structure, the frequency response function will be completely different [12]. By concentrating the entire force spectrum at a single frequency, sinusoidal excitations can produce the highest possible response levels for a given force rating of the exciter [13]. As a result, individual modes can be tuned and studied at controlled amplitude levels. This testing method is highly desirable in the nonlinear situations due to slippage or friction, rattling or loose components [14].

Figures 11 and 12 show the lowest two modes for the $L4$ and $L10$ panels as a function of the vibration amplitude, respectively. In the abscissa the measured vibration amplitude is normalized by the panel thickness, whereas in the ordinate

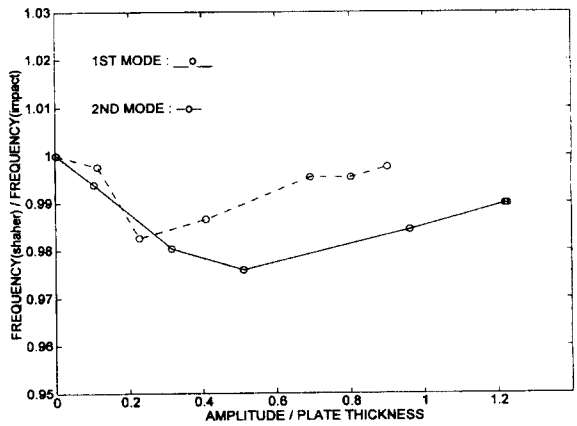

Fig. 11 Normalized first and second natural frequencies of the $L4$ panel versus normalized vibration amplitude.

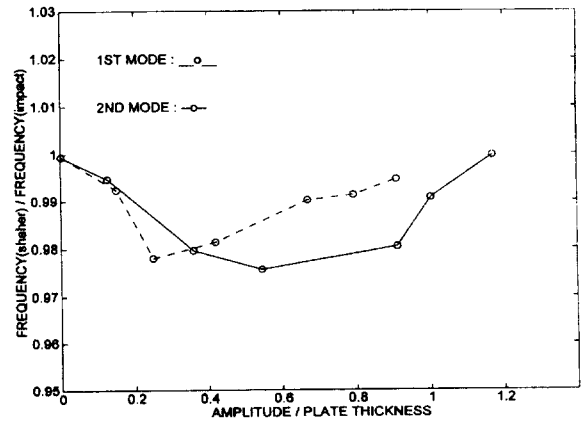

Fig. 12 Normalized first and second natural frequencies of the $L10$ panel versus normalized vibration amplitude.

the measured natural frequency is normalized by those obtained with the hammer test. At first a moderate drop in frequency is observed by maximum 3 % for the first mode and 2 % for the second mode. The decrease in frequency is considered as a softening effect: *i.e.*, relative motion between parts of the joint starts due to the looseness with the increasing amplitude. This fact makes frequencies lower. Frequencies then start to rise at a certain amplitude. The increase in frequency is considered as a stiffening effect: *i.e.*, as the relative motion reaches maximum allowed by the hole clearance, membrane stresses of the increased amplitude results in rising effective panel stiffness due to clamped boundary conditions. Minimum frequency obtained by the shaker test should be a reliable design parameter to be compared with numerical predictions.

6. Measurement of Modal Parameter Sensitivity

Modal properties for the double *CC* beam were theoretically observed to be very sensitive to the stiffnesses of midspan torsional and translational springs. This analytical approach provides a means of experimental measurements for these stiffnesses. Modal parameter sensitivities are first measured experimentally, and then the corresponding stiffnesses are estimated using computational tools.

6.1 Natural Frequency

Natural frequencies analytically measured by an introduction of infinite stiffness can be used as bases for experimental natural frequencies of the *LRV* beam. Since the lap joint beam actually has an overlapping material mass at midspan, natural frequency bases for the *LRV* beam are completely different from those of the simple *CC* beam.

Table 2 Bases for natural frequencies for simple and jointed beams (Hz).

Mode / Sample	1	2	3	4	5	6
CF	45.51	285.26	799.15			
CC	72.41	199.60	391.33	647.09	967.09	1351.90
LRV	69.07	199.53	378.05	646.41	935.54	1349.00

Table 3 Natural frequency sensitivities for the lap joint beam due to the torsional and the translational stiffness.

Mode / Test	Elastic restrantin (Hz)			Elastic support (Hz)		
	1	3	5	2	4	6
Test I	67.21	357.40	847.70	199.80	632.80	1218.70
Test II	68.00	361.30	849.20	199.00	624.60	1220.40
Test III	69.39	363.40	860.30	198.70	633.50	1244.00
Average	68.20	360.70	852.40	199.20	630.30	1227.70
Base	69.07	378.05	935.54	199.53	646.41	1349.00
Sensitivity	-1.26%	-4.59%	-8.89%	-0.17%	-2.49%	-9.00%
Stiffness	G = 13.37			K = 1066.41		

$1G$ = 0.730 kgf/m, $1K$ = 19.358 kgf/m

This structural difference resulted in numerical extractions of natural frequency bases for the lap joint beam.

The values listed in Table 2 were calculated using finite element analysis tools, PATRAN and ABAQUS. Beam elements with a cubic interpolation were used in modeling of the *LRV* beam. The beam element has no shearing effect based on classical Euler-Bernoulli assumptions. Midspan stiffnesses were controlled by spring elements which are simple linear springs acting between two nodes in a fixed direction or rotation.

As previously presumed for an added mass effects, values of natural frequencies for symmetric modes were found lower than those of the *CC* beam because of mass participations in the vibration cycle. On the other hand, no significant difference for anti-symmetric modes is observed because the joint mass only contributes rotary inertia. Table 3 lists the averaged frequencies and the corresponding sensitivities

based on reference frequencies presented in table 2. Figures 13 and 14 show predictions of stiffness values by locating experimentally measured frequency sensitivities on the sensitivity curve and then reading those corresponding nondimensional stiffnesses, G = 13.77 and K = 1066.41, respectively. Finally, using equations (7) and (8), nondimensional stiffnesses were converted to obtain actual torsional stiffness k_t = 10.68 kgf/m and translational stiffness k_t = 20644 kgf/m, respectively.

6.2 Tip Deflection

The consistent mode shape amplitude for the reference, *CC* or *CF*, and the *LRV* beams should be obtained by force levels applied in the linear range of 'ankylosis' as stated earlier. Deflections were measured at the midspan location where those for symmetric modes are maxima. Note that deflections of the *LRV* beam at the midspan for anti-symmetric modes are not zero due to the joint flexibility. Therefore, midspan deflections for anti-symmetric modes has real sensitivities to those of the reference *CF* beam. Bases for experimentally measured deflections and averaged deflections are given by Table 4. Values of the torsional and the translational stiffness for the *LRV* beam can be estimated from Figs.

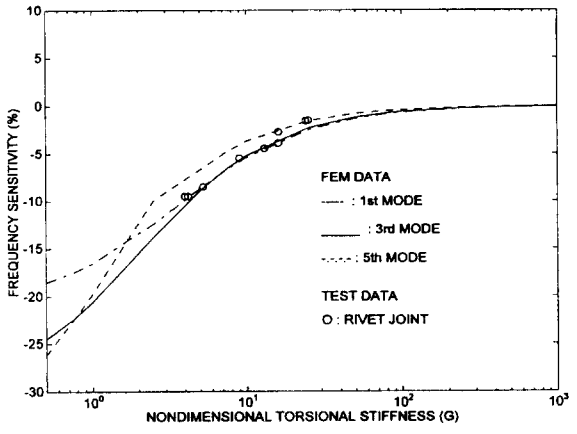

Fig. 13 The natural frequency sensitivity in lap joint for the prediction of torsional stiffness.

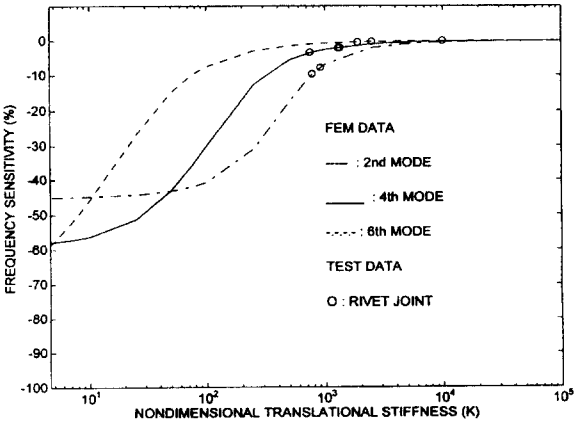

Fig. 14 The natural frequency sensitivity in lap joint for the prediction of translational stiffness.

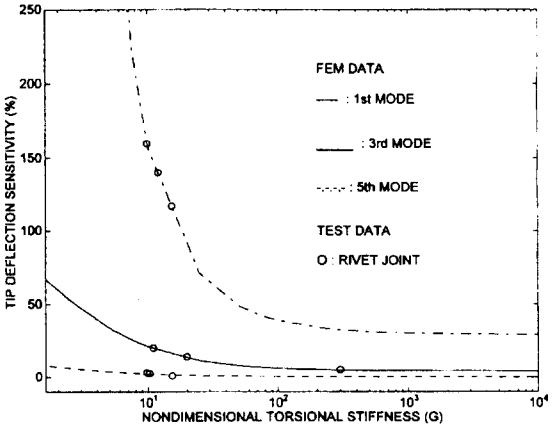

Fig. 15 The tip deflection sensitivity in lap joint for the prediction of torsional stiffness.

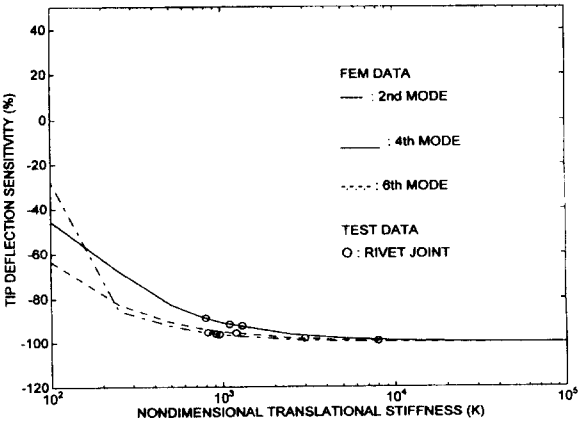

Fig. 16 The tip deflection sensitivity in lap joint for the prediction of translational stiffness.

Table 4 Experimentally measured tip deflections and bases for the lap joint beam $[10^{-2}$ mm].

Mode / Test	1	2	3	4	5	6	K	G
LRV	25.832	0.584	28.702	2.286	60.960	1.016	1012.30	12.82
BASE	26.238	30.734	32.944	62.408	53.873	253.721	0	∞

$1G$ = 0.730 kgf/m, $1K$ = 19.358 kgf/m

Table 5 Summary of joint stiffness estimates based on sensitivity measurements for frequencies and tip deflections.

Sensitivity \ Stiffness	Translational (K)	Torsional (G)
Frequency	1066.41	13.37
Tip deflection	1012.30	12.82
Average	1039.36	13.10

$1G$ = 0.730 kgf/m, $1K$ = 19.358 kgf/m

Table 6 The MAC matrix for the $L4$ panel modeled using the *BM-RF* method.

Mode	1	2	3	4	5
1	0.99	0.00	0.00	0.00	0.05
2	0.00	0.99	0.00	0.00	0.00
3	0.00	0.00	0.91	0.03	0.00
4	0.00	0.00	0.03	0.92	0.00
5	0.06	0.05	0.00	0.01	0.80

Table 7 The MAC matrix for the $L10$ panel modeled using the *BM-RF* method.

Mode	1	2	3	4	5
1	0.99	0.00	0.04	0.00	0.04
2	0.02	0.97	0.00	0.00	0.01
3	0.00	0.00	0.98	0.01	0.00
4	0.00	0.00	0.01	0.96	0.00
5	0.15	0.00	0.00	0.00	0.98

15 and 16, respectively.

Finally, values necessary for the finite element implementation were predicted by averaging a collection of stiffnesses from readings of different modal parameter sensitivities, as summarized in Table 5. Damping levels were experimentally observed below 1 % critical and have a little effect on natural frequencies. This low damping level implies that the joint can be modeled by only spring elements without any damping element.

7. Modeling Technique

7.1 Conventional Modeling Method

It should be noted that no clear guideline is available for modeling fastened joints. The existing method will mimic a rigid modeling technique used for modeling connected regions. Those regions were also dimensionally simplified to a collection of one or two dimensional element configurations by adjoining them rigidly to adjacent skins by means of shared nodes. Therefore it is anticipated that this method results in overestimates of frequencies. For simulating this modeling approach for lap joint panels, $L4$ and $L10$, the joint was replaced with a reinforcing beam located at the geometric centroid of the connected region. A line of reinforcing beam shared nodes with the centroid in the finite model. Figure 17 shows this *beam reinforcement* method denoted as *BM-RF*. The sectional area and inertial property of the beam were adjusted to represent the transverse stiffening effect of the splice plate.

Figure 18 shows the correlation between measured and predicted frequencies. The

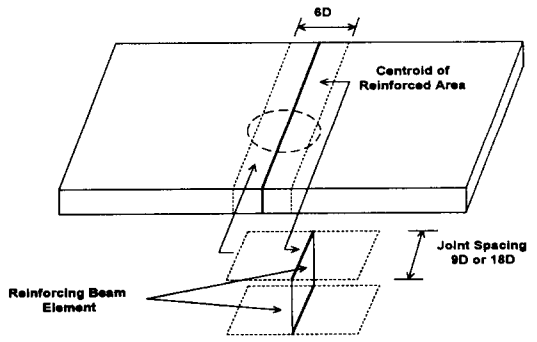

Fig. 17 The beam reinforcement (BM-RF) element method.

BM-RF method systematically overestimates frequencies by about 20 % which is caused by the infinite increase in stiffness of the joint. The MAC matrix for the *L4* panel is listed in Table 6. The diagonal values of the MAC matrix are above 0.90 except for the fifth mode with a 20 % error. Table 7 presents the corresponding data for the *L10* panel. The diagonal elements are above 0.95, thereby indicating an excellent correlation between measured and predicted mode shapes. Measured damping ratios were less than 2 % for test samples.

In summary, the predicted mode shapes are in general satisfactory, even though the frequency correlation is rather poor. Mode shapes do not play a significant role in detecting modeling errors. Due to very low damping levels, finite element models without damping elements can be achieved for controlling frequencies. As a result, modeling error sources can be considered as conservatively rigid connections relevant unknown type and unknown magnitude of the joint stiffness.

As shown in Table 5, translational and torsional stiffness, K and G, were experimentally measured by modal parameter sensitivities for a single lap joint beam. However, it does not indicate that these measured values can be directly applied to multi-dimensional structures, primarily because for each mode of dimensionally complicated structures the type of force such as translational force, bending or torsional moment acting in the joint is quite difficult to identify. This question arises as to how to utilize joint stiffnesses measured in the one dimensional structure and implement those values into finite element models of the joint on the multi-dimensional structure.

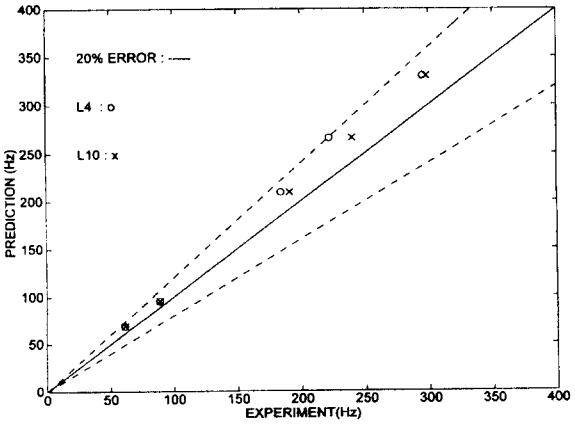

Fig. 18 Correlation between measured and predicted frequencies for *L4* and *L10* panels using the BM-RF method.

7.2 Test Data Applicability

In general, higher vibration modes are influenced by a combination of translational force and bending moment in many unknown directions. Forces are complicatedly coupled in higher modes. However, for lower modes a fewer type of forces tend to be dominant in one direction. The stiffness values measured from the lap joint beam can not provide the capability of its direct implementation in the finite element model of the jointed panel, because there still exist unknown magnitudes of forces acting in unknown directions. Furthermore, it is very difficult to predict a unique value of stiffness in a specified direction, independent of the influence on other forces [15,16]. An important implication of the measured joint stiffness is that the measured value can be maximum magnitude in one direction of the multi-dimensional structure with various joints.

Implementations of the translational spring constant k_t and the torsional spring constant k_l in the finite element analysis cause great difficulties in controlling an independent stiffness in each direction. In fact, a different element type is needed as a substitute for the spring element which has a lack of dimensional versatility. The beam element with circular cross-section takes better advantage of performing characteristics of heavily coupled forces. By controlling the

beam element diameter, d_e, rather than the magnitude of each spring constant in three independent directions, the number of design variables to be used in the numerical model can be reduced to only one. Furthermore, the circular cross-section of the beam element provides better capabilities for translational forces and moments around the circumference of the joint. The beam element can be positioned at the joint location. Hence, a very small length of beam element is necessary for modeling the joint. As the beam becomes shorter, the effect of shear deformation becomes so evident that the use of the Timoshenko beam element is desirable in the finite element analysis. The transverse shear deformation in this beam element is treated as if the response were linear elastic, independent of the axial and bending responses.

7.3 Proposed Finite Element Model

Figure 19 shows the refined model of the connected region. The fastener is represented by a perimeter of beam elements around the fastener hole. Each plate is represented by its center plane and beam elements are connected by sharing nodes on two disjointed plates. To investigate effects for the number of beam elements to be implemented into joints, n beam elements are used in the model. In the present work, the simplest model, $n = 1$, uses a single beam element at the center of the joint; the other two models, $n = 4$ or $n = 8$, have four or eight beams equally spaced around the perimeter of the fastener hole, respectively.

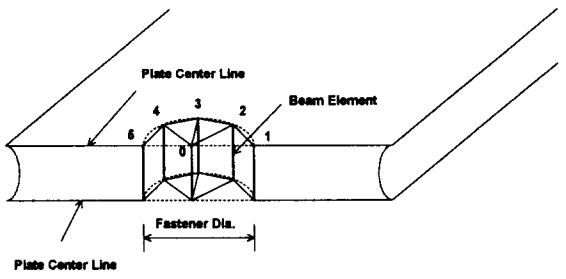

Fig. 19 A schematic diagram of the finite element model in the joint area.

It is very difficult to identify the prying action and its value[17]. As a result, the position and stiffness magnitude for the prying contact, independent of the joint flexibility, are still unknowns. This effect was incorporated into the stiffness of the beam element. The mass properties of beam element were calculated to match the total fastener mass.

Finite element models were made using the PATRAN and ABAQUS packages. The effects of discretization idealization errors on the model were observed for the simple plate by increasing the element size (h-refinement) and also by increasing the element order (p-refinement)[18]. Panels were modeled with four noded and shear deformable plate elements meshed by 1.62 cm^2. Discretization errors were less than 1 % for the first five modes. But, the modeling of fastener regions was produced by the paver type mesher required more sufficient discretizations for the bulk of the plate elements.

7.4 Design Data Implementation

Experimental stiffness values from a single joint beam were assumed as maximum values in an unknown direction in the fastened panel. At first, maximum beam size should be determined according to an individual force influence. After the limited values of the beam diameter are set up as lower or upper bounds associated with each force effect, changes in diameter will be made possible to tune frequencies. The bound of the beam size will be calculated by determining the force type being transferred across the joint.

Lap joints are subjected to a bending moment M acting in an unknown direction, a shear force acting in a direction normal to the plane of the panel, and an axial

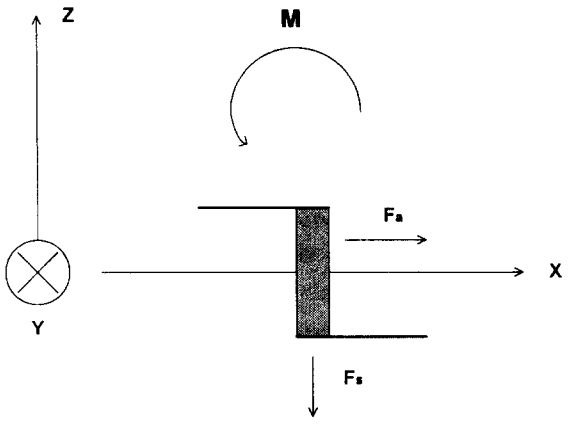

Fig. 20 A schematic diagram of the forces acting in the lap joint.

force acting in the plane of the panel. In other words, referring to a schematic diagram of Fig. 20, the shear force F_s acts in a direction parallel to the fastener axis, whereas the axial force F_a acts in a direction transverse to the fastener axis. First, if an assumption is made that the structure is under sole bending moments and n beam elements are equally spaced around the joint in the fastener's direction, the experimentally measured stiffness k_t is equivalent to the sum of each torsional stiffness of the beam element used in the model. Therefore, an equivalent torsional stiffness of the beam element yields the following relationship:

$$n\frac{E_e I_e}{\ell_e} = k_t \tag{11}$$

where $I_e = \pi d_e^4/64$ is the second area moment of the beam's cross-section, E_e is Young's modulus of the fastener material, d_e the beam element diameter and ℓ_e its length, 2.29 mm.

Next, a similar reasoning can be applied to the effect of sole translational forces in n beam elements followed by an equivalent translational stiffness

$$n\frac{E_e A_e}{\ell_e} = k_v \tag{12}$$

where $A_e = \pi d_e^2/4$ is the element cross-sectional area. From the equivalent stiffness relationships, equations (11) and (12), the beam element size in mm can be calculated as follows:

for the sole bending moment effect M:

$$d_e = 85.2983 \sqrt[4]{\frac{G}{nE_e}} \tag{13}$$

for the sole shearing force effect F_s:

$$d_e = 8.9510\sqrt{\frac{K}{nE_e}} \tag{14}$$

where nondimensional torsional stiffness G and nondimensional translational stiffness K were defined in equations (7) and (8), respectively.

The beam diameter d_e is proportional to the stiffness and inversely proportional to the number of beam elements. The estimated joint stiffnesses listed in Table 5 are used

Table 8 Beam element diameter d_e [10^{-2}mm] estimated from the measured joint stiffnesses.

n	Based on G	Based on K
1	279.4	8.9
4	200.7	4.3
8	170.2	3.0

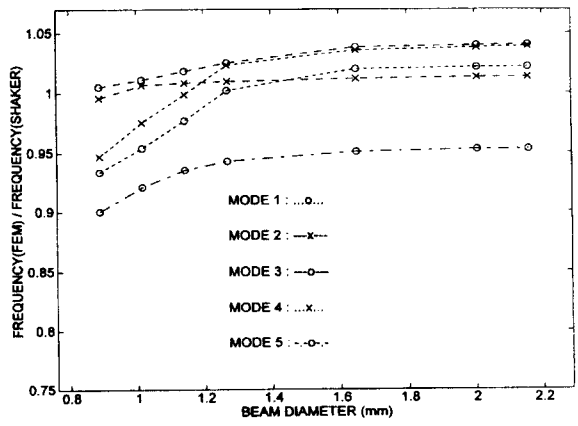

Fig. 21 Normalized frequencies versus d_e for the $L4$ panel (n = 4).

to compute beam diameters using equations (13) and (14). Table 8 lists the results for different values of n. Young's modulus of the rivet was 7.312×10^9 kg/m^2.

These values can be fine-tuned based on the experimentally measured frequencies using the shaker test. Figure 21 shows the normalized frequencies for the $L4$ lap joint panel as a function of beam diameter, for $n = 4$. Frequencies computed by the finite element model are normalized by experimentally measured frequencies. Beam diameter variations, d_ϵ, are made from 0.889 to 2.159 mm. The lower and upper bounds from table 8 are 0.043 and 2.007 mm, respectively. Predicted frequencies calculated with d_ϵ above the upper bound are almost independent of d_ϵ. For d_ϵ values below 1.270 mm, frequency discrepancies become significantly large. The best correlation occurs approximately at the value d_ϵ = 2.032 mm. Therefore, the beam element diameters calculated from the measurements of joint stiffnesses provide likely range values for tuning frequencies.

Similar behaviors can be observed for other finite element configurations as shown in Figs. 22, 23 and 24 for the $L4$ model with $n = 8$, and the $L10$ with $n = 4$ or $n = 8$, respectively. Table 9 lists the values of n and d_ϵ yielding the best correlation with experimentally measured frequencies for those corresponding finite element models. Within estimated bounds of beam diameter for all numerical models, the lowest three predicted frequencies tend to be in better agreement with the

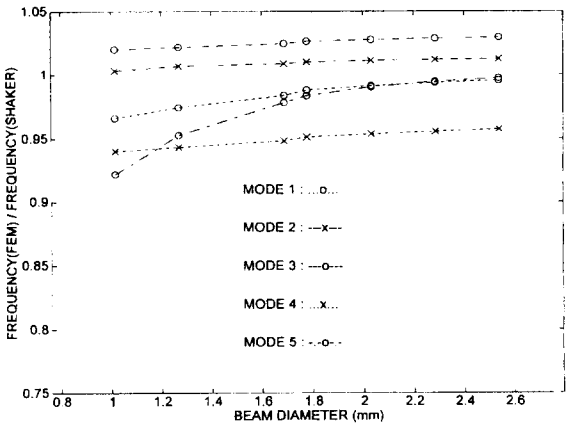

Fig. 22 Normalized frequencies versus d_e for the $L4$ panel ($n = 8$).

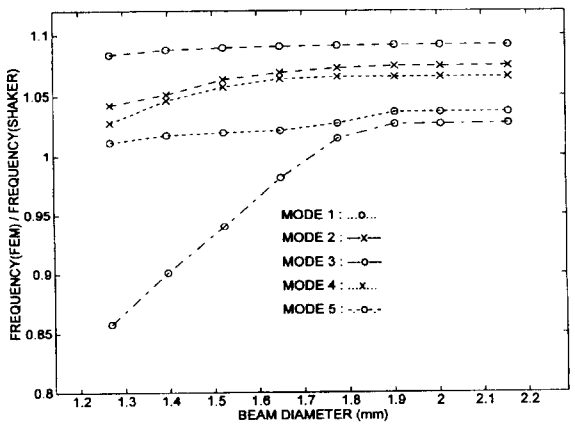

Fig. 23 Normalized frequencies versus d_e for the $L10$ panel ($n = 4$).

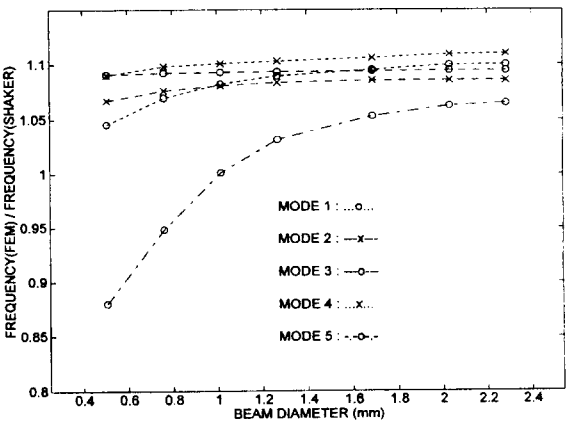

Fig. 24 Normalized frequencies versus d_ϵ for the $L10$ panel ($n = 8$).

Table 9 Model parameters, n and d_ϵ [10^{-2}mm], for lap joint panels.

Sample	n	d_e
$L4$	4	200.7
	8	170.2
$L10$	4	177.8
	8	101.6

measurements and has little effect on beam diameter. This physical phenomenon would indicate that the beam diameter predicted by any joint stiffness measurement yield good correlations with the lowest measured frequencies. Fine-tuning only improves the correlation for the last two modes. It should be noted that for the lap joints, the optimal value of d_e is close to that extracted from the measured joint torsional stiffness G.

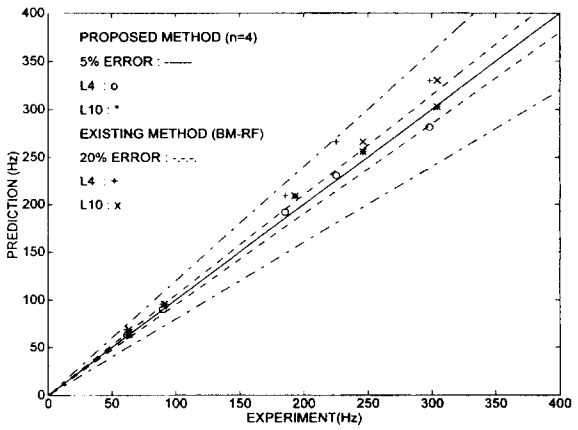

Fig. 25 Correlation between measured and predicted frequencies for $L4$ and $L10$ panels using the BM-RF and proposed finite element models (n= 4)

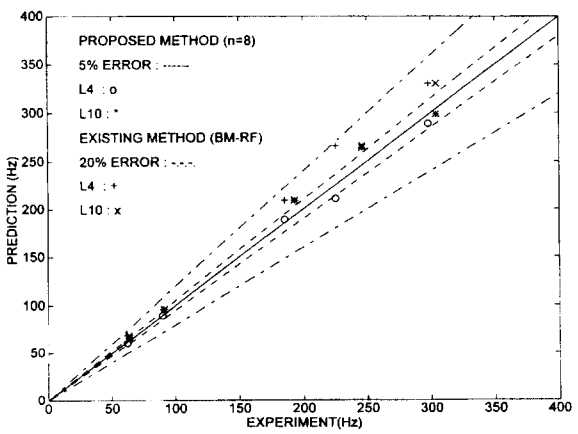

Fig. 26 Correlation between measured and predicted frequencies for $L4$ and $L10$ panels using the BM-RF and proposed finite element models (n= 8)

7.5 Comparison with Conventional Approach

The frequencies predicted by the proposed finite element model will be compared with the measured frequencies described in the previous section. Table 9 lists design parameters of finite element models. Figure 25 shows that experimentally measured frequencies are compared with those predicted by the proposed $L4$ and $L10$ models of n = 4 and those estimated by the *BM-RF* method, respectively. Errors of up to 20 % are observed for the *BM-RF* methods, but are reduced to 5 % for the proposed model. Similarly, the results for n = 8 are shown in Fig. 26. Errors are reduced from 20 % for the existing method to 5 % for the proposed model.

8. Conclusion

This paper describes a combination of experimental and analytical investigation aimed at identifying modeling errors, accounting for the lack of correlation between experimental measurements and analytical predictions of the modal parameters for lap joint panels. Large discrepancies were observed between measured and predicted natural frequencies that can be almost entirely ascribed to the conservative modeling method.

Based on this experimental evidence, improved finite element models of the joint were developed using a set of concentrated translational and torsional spring constants experimentally determined in a single lap joint. The implementation of these experimentally determined joint stiffnesses is not a straightforward process because some types of forces such shear force, axial force and bending moment are complicatedly coupled and different from mode to mode. However, these stiffness values provide a means of the bounds, within which design parameters can be fine-tuned to match experimental results. The spring element has a lack of

dimensional versatility and is replaced by the beam element. In the proposed finite element model, the joint flexibility is represented by beams with a circular cross-section which diameter is evaluated from the measured joint stiffnesses.

The frequencies predicted by this proposed numerical model were compared with the measured frequencies using the shaker test. The predictions based on this new model are considerably better than those based on conventional modeling practices: errors of up to about 20 % obtained with the *BM-RF* methods were reduced to about 5 % with the proposed methodology.

Finally, the proposed finite element model may require expensive computations for refined representations of the joint area, but the joint DOF will be greatly reduced because the joint is expressed as a lumped parameter. As a result, this design parameter would be universally used for the same type of joints.

References

(1) Bortman, J. and Szabo, B. A., 1992, "Analysis of Fastened Structural Connections," AIAA Journal, Vol. 30, pp. 2758~2764.

(2) Barrios, W., 1978, "Stress and Displacements due to Load Transfers in Structural Assemblies," Engineering Fracture Mechanics, Vol. 10, pp. 115~176.

(3) Good, M. R. and Macioce D. J., 1984, "Using Experimental Modal Analysis to Characterize Automobile Body Joints and Improve Finite Element Analysis," Proceedings of the 2nd International Modal Analysis Conference, Orlando, Florida, pp. 106~110.

(4) Ankara, A. and Dara, G., 1994, "Analysis of Structural Lap Joints in Metals, Material & Design," Vol. 15, pp. 159~163.

(5) Sawa, T., Kumano, H. and Morohoshi, T., 1996, "The Contact Stress in a Bolted Joint with a Threaded Bolt," Experimental Mechanics, Vol. 36, pp. 17~23.

(6) Twomey, W. J., 1992, "The NASA/Industry Design Analysis Method for Vibrations (DAMVIBS) Program-Sikorsky Aircraf- Advances toward Interacting with the Airframe Design Process," AIAA/ASME/ASCE/AHS 33rd Annual Structures, Structural Dynamics and Material Conference, Dallas, Texas, pp. 1149~1158.

(7) Wong, K. and Firman, A., 1985, "Concept, Technique and Experience in the Idealization of Car body Structure for Finite Element Analysis," Conference Publications on Railway Vehicle Body Structures, London, pp. 37~44.

(8) Baruch, H. and Khatri, M. P., 1987, "Identification of Modal Parameters in Vibrating Structure," Proceedings of the AIAA/ASME/ASCE/AHS 28th Annual Structures, Structural Dynamics and Material Conference, New York, pp. 152~162.

(9) Nagy, E. J., 1981, "Improved Method in Ground Vibration Testing," American Helicopter Society Specialists Meeting on Helicopter Vibration, Print No. 81-6, Hartford, Connecticut.

(10) PATRAN Users Guide, 1994, PDA Engineering, Costa Mesa, California.

(11) ABAQUS/Standard Users Manual, Vol. I, 1994, Hibbit, Karlsson & Sorensen Inc., Pawtucket, Rhode Island.

(12) Olsen, N., 1985, "Excitation Functions for Structural Frequency Response Measurement," Proceedings of the 3rd International Modal Ana- lysis Conference, Orlando, Florida, pp. 894~902.

(13) Ramsey, K. A., 1976, "Effective Measurements for Structural Dynamic Testing (Part II)," Sound and Vibration, Vol. 10, 18~31.

(14) Bubsy, H. R., Nopporn C. and Singh R., 1986, "Experimental Modal Analysis of Nonlinear Systems: A Feasibility Study," Journal of Sound and Vibration, Vol. 180, pp. 415~457.

(15) Maruyama, K., Yoshimoto I. and Nakano, Y., 1975, "On Spring Constant of Connected Parts in Bolted Joint," Bulletin of JSME, Vol. 18, pp.126.

(16) Jinsong, T. and Zhaoyi, D., 1988, "Better Stresss and Stiffness Estimates for Bolted Joints," Machine Design, Vol. 60, 114~119.

(17) Chasten, C. P. and Lu, L. -W., 1992, "Prying and Shear in End-Plate Connection Design," Journal of Structural Engineering, ASCE, Vol. 118, 1295~1311.

(18) Hughes, T. J. R., 1987, The Finite Element Method: Linear Static and Dynamic Finite Element Analysis, 4th Edn. Prentice- Hall, New Jersey.